Nonlinear analysis to investigate effect of connection type on behavior of steel plate shear wall in RC frame

Maryam Bypour*[1], Majid Gholhaki[2], Mahdi Kioumarsi*[3], Benyamin Kioumarsi[4]

[1]M.Sc. Graduate of Structure Engineering, Faculty of Civil Engineering, Semnan University, Semnan, Iran (mbypour@alum.semnan.ac.ir)

[2]Associate Professor, Faculty of Civil Engineering, Semnan University, Semnan, Iran (mgholhaki@semnan.ac.ir)

[3]Associate Professor, Department of Civil Engineering and Energy Technology, OsloMet – Oslo Metropolitan University, Oslo, Norway (mahdi.kioumarsi@hioa.no)

[2]PhD Student, Faculty of Civil Engineering, Semnan University, Semnan, Iran (benyamin.kioumarsi@gmail.com)

Abstract

In the reinforced concrete (RC) structures with steel plate shear walls (SPSWs) as a lateral load resisting system, to obtain maximum capacity of SPSW, implementing proper connections play an important role to transfer force from wall to the frame. In this paper, four connection types are proposed and numerically investigated to transfer the tension field forces between SPSW and RC frame (RCF). Three types of connections are applicable for rehabilitating of existing RC structures and one type can be used for new construction. The behavior of connections has been evaluated using non-linear finite element analysis (NLFEA). Results of the specimens with different types of connections demonstrated that the use of SPSW in RCF with appropriate connections could provide excellent ductility as well as high load carrying capacity and initial stiffness by distributing the yielding zone in SPSW along the wall height.

Keywords: Steel Plate Shear Wall (SPSW), Reinforced concrete, Rehabilitation, Behavior factor, Connections.

1. Introduction

After the 1994 Northridge Earthquake and the 1995 Kobe Earthquake where significant structural damages were observed, seismic design requirements of structures were changed fundamentally. It was observed that the designed buildings according to the previous versions of the earthquake codes have inadequate resistance due to the lack of technical knowledge and the use of poor quality materials [1]. In addition, buildings, which were designed only for gravity load as well as the buildings whose applications are changed need to be retrofitted.

Different methods are used to retrofit the existing reinforced concrete (RC) structures [2-5]. One of the methods is to use conventional braces (CBs). Although the use of the CBs systems has been practiced for decades for the rehabilitation of RC structures [6-8], the unbalanced hysteresis behavior of the CBs system tends to result in damage concentration in specific stories [9]. For this reason, the use of buckling-restrained braces (BRBs) that can increases the structural integrity and reduce the seismic response of structures by energy absorption, is considered as an effective way to improve the seismic performance of RC structures [9-11]. The use of steel and concrete jacketing and carbon fiber reinforced polymer (CFRPs) for the rehabilitation of RC structures efficiently increases ductility, energy dissipation capacity and the maximum strength [12-14].

In the recent decades, Steel Plate Shear Walls (SPSWs), whose design criteria are presented in AISC [15] and CSA [16] codes, have been used as a lateral loads resisting system in buildings, especially in high-rise buildings [17, 18]. The results of experimental tests conducted on SPSWs indicated significant stiffness, load carrying capacity, ductility and energy dissipation in these lateral load resisting systems [19-25]. In the experimental study carried out by Chen et al. [26] for the rehabilitation of existing RC structures, SPSW with LYP100 steel was used. Fig. 1(a) shows the connection details of SPSW to RC frame (RCF) in the study. As shown in this figure, SPSW were connected to RCF by H-shaped steel frame (SF) working on its weak axis. SF was attached to RCF by chemical anchors and shear bolts designed to efficiently transfer shear force. Spiral stirrups were placed inside the mortar fill for better performance of

the connection between the SF and RCF. The results demonstrated that with proper design and fabrication, the steel shear panel made of LYP steel was able to achieve significant energy dissipation capacity.

In the experimental study of Formisano et al. [27], rehabilitation of RC structures was conducted using steel and aluminum shear panels. As shown in Fig. 1(b), SPSWs have been connected to RCF by U-shaped section and bolts. The result demonstrated that the rehabilitation of RC structures by the steel and aluminum shear panels could be considered as an effective strengthening and stiffening device that is able to significantly increase the energy dissipation capacity of existing RC structures. Choi and Park [28] conducted an experimental study for investigating thin SPSW performance in RCF. In this study, RCF was experimentally compared with RC shear walls. For connecting SPSW to RCF, as shown in Fig. 1(c), two rows of studs welded to the end plates have been used. SPSWs have been welded to the end plates by fish plates. The test results demonstrated that the use of SPSW in RCF provided large initial stiffness, load carrying capacity, ductility and energy dissipation. Furthermore, shear cracking at the beam-column joints in the RCF have been prevented. Comparison of the result showed that RCF accompanied by SPSW has better ductility, energy dissipation and failure mechanism compared to those of RCF accompanied by RC shear wall. In an experimental study conducted by Gorgulu et al. [29], the performance of external steel shear walls (SSW) in RCF was investigated. SSW was designed as an inverted V brace and the external frame was connected to RCF using bolts. The connection details is shown in Fig. 1(d). The results demonstrated that external SSW increases load-carrying capacity and lateral stiffness. No damage has been occurred in the bolts since the forces have been transferred well to the RCF.

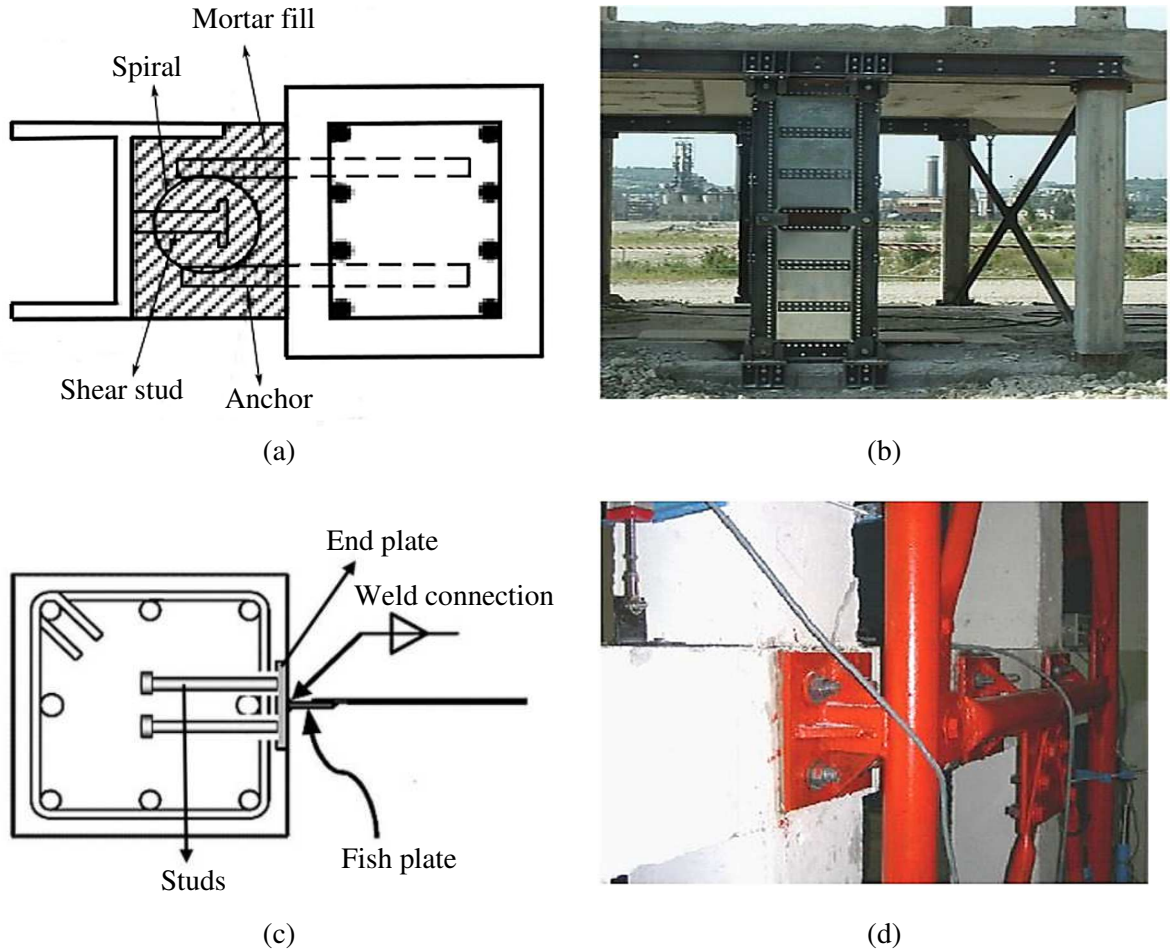

Fig. 1 Details of SPSW to RCF connections in the previous experimental studies: a) H-shaped steel frame connection, by Chen et al. [26], b) connection using UPN profiles and bolts, by Formisano et al. [27], c) connection using two rows of studs welded to the end plates, by Choi and Park [28] and d) connection using bolts by Gorgulu et al. [29].

Choi and Park [28], to verify of their experimental results of SPSW in RCF, conducted nonlinear push-over analysis with Opensees software. In this study SPSW were modeled as a series of inclined pin-ended tension strips. In this numerical models truss element for SPSW and nonlinear Beam- Column element for RCF were used. The load-carrying capacities and initial stiffness of numerical model have been indicated good agreement however load-carrying capacities value of numerical models were smaller than the test result because the strain-hardening effect of the steel subjected to cyclic loading was not considered.

Gorgulu et al [29] to modeling of SSW in RCF were carried out nonlinear static analysis by SAP2000 software. In the numerical model, the effective stiffness of the sections was taken as 0.4EI for the beams and the columns and the plastic hinges were defined at the ends of the structural elements. This FE models

satisfactorily approximated the post-yield behavior of SSW in RCF. In this study, some overestimations were reported for the linear elastic region. This overestimation could be controlled by lowering the effective section stiffness of the RC columns under low levels of axial load.

An important issue in the rehabilitation of RC structures with SPSW is to provide proper connection between SPSW and RCF, such that the boundary members have sufficient rigidity to transfer the tension field forces of SPSW to RCF. In this work, since the performance of different methods of connecting SPSW to RCF and the affecting parameters on connection performance, are barely investigated, four proposed connections for connecting SPSW and RCF are investigated. Three connection types are for the rehabilitation of RC structures and one type is for new construction. The main objective of this work is to get an opportunity to assess existing experimental test data for non-linear finite element analysis (NLFEA) to obtain realistic prediction of behavior of proposed connection using the commercially available finite element program ABAQUS. To obtain the optimized connection, using NLFEA, a parametric study is conducted to compare the performance of the proposed connections.

2. Finite element analysis

2.1 Selected experimental case

In this study, the experimental investigation of Choi and Park [30] have been used for verification of nonlinear finite element (NLFE) model with ABAQUS 6.14-5. The specimen tested in the investigation was one-third scale specimens of three-story RCF with SPSW. Dimensions and reinforcement details of the selected experimental case (SPIW1 specimen) are illustrated in Fig. 2(a). Detail of the cross-sections of beam and columns are shown in Figs. 2(b)-(c), respectively. In this experimental study to transfer the forces between SPSW and RCF, studs were embedded in the columns and beams, see Fig. 1(c). The design forces for the studs were estimated by assuming that the tension field forces of the steel infill plate are uniformly distributed along the boundary frame. Two rows of studs (diameter = 13 mm, length = 150 mm)

were welded to the end plates (width = 100 mm, thickness = 12 mm) at intervals of 100 mm. The SPSW was weld-connected to the end plates by fish plates (width = 50 mm, thickness = 6 mm).

The boundary frame was designed as a special RCF in accordance to building code requirements ACI 318-08 [30]. The thickness of the steel infill plates was 2 mm and its aspect ratio (l_p/h_p) was 1.5 ($l_p = 1{,}500$ mm and $h_p = 1{,}000$ mm, where l_p and h_p are the length and height of the steel infill plate, respectively).

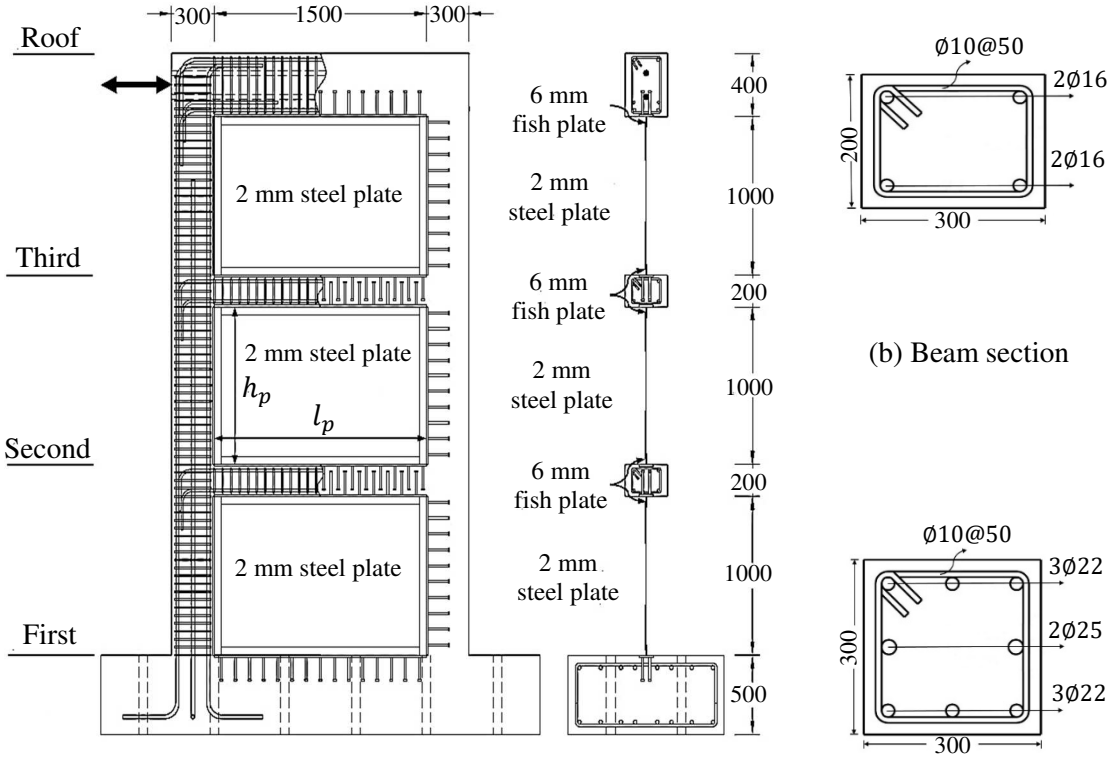

Fig. 2 Details of experimental RCF with SPSW test (mm) [28]

2.2 Simulation and analyzing

Full 3D nonlinear static analysis was carried out. The loading process was controlled by displacement at the top beam. A displacement equal to the maximum target displacement of experimental test was applied in NLFEA. The Newton-Raphson iterative approach was selected to solve the non-linear problem. To model the SPSW, 4-node shell element with reduced integration (S4R) is used. This element is used for both thick and thin shells. For modeling the concrete and connection plates, 8-node solid element with

reduced integration (C3D8R) is used. Truss elements (T3D2) are used for modeling reinforcements and studs. To define the interaction between concrete and reinforcements as well as concrete and studs, embedded region interaction is used. To define interaction between concrete and end plates, surface-to-surface contact interaction is used. Normal and tangential behavior are considered in the interaction element. To define connection between studs and end plates as well as SPSW-fish plate connection, Tie constraint is used. The FE model of the connections, meshing size and boundary conditions are shown in Figs. 3(a)-(c). As shown in Fig. 3(c) displacement and rotations in foundation are limited in three direction and displacement is applied in top beam.

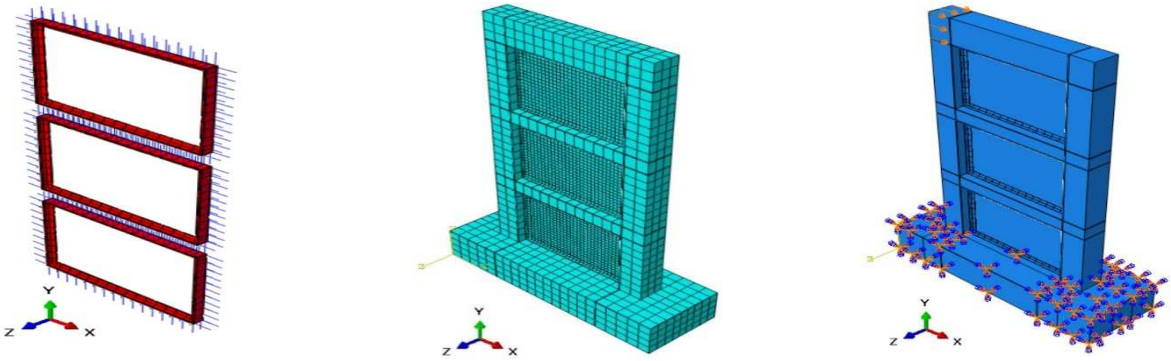

(a) Connections (b) Meshing size (c) Boundary conditions

Fig. 3 FE model of SPSW and RCF in ABAQUS

2.3 Material properties

In the simulation of the experimental specimen, all defined material properties are obtained from the experimental study. The modules of elasticity and compressive strength of concrete for the experimental specimens are 25000 and 26.4 MPa, respectively. For simulation of concrete behavior, Concrete Damage Plasticity (CDP) model was used. The CDP model assumes that the concrete failure in tensile cracking and compressive crushing is characterized by damage plasticity. The employed parameters of CDP model for concrete are presented in Table 1. In this Table, Ψ is the dilation angle measured in the p–q plane at high confining pressure, $\in$ is a parameter, referred to as the eccentricity, f_{b0}/f_{c0} is the ratio of initial equibiaxial compressive yield stress to initial uniaxial compressive yield stress and K_c is the ratio of the second stress invariant on the tensile meridian [31].

Table 1 Material parameters of CDP model for concrete

Dilation angle (Ψ)	Eccentricity (ϵ)	f_{b0}/f_{c0}	K_c	Viscosity Parameter
31	0.1	1.16	0.67	0.002

As it presented in Fig. 4 and according to ABAQUS/Standard 6.14, the stress–strain curves for uniaxial tension and compression must define elastic, plastic and damage behaviors of concrete. Eq. 1(a)-(b) show the concrete behavior to uniaxial loading in tension and compression respectively. The stress–strain relations under uniaxial tension and compression are [31].

$$\sigma_t = (1 - d_t)E_0\left(\varepsilon_t - \tilde{\varepsilon}_t^{pl}\right) \qquad (1a)$$

$$\sigma_c = (1 - d_c)E_0\left(\varepsilon_c - \tilde{\varepsilon}_c^{pl}\right) \qquad (1b)$$

where E_0 is the initial elastic stiffness of the concrete, d_t and d_c are the uniaxial damage variables for tension and compression, respectively, $\tilde{\varepsilon}_t^{pl}$ and $\tilde{\varepsilon}_c^{pl}$ are the tensile and compressive equivalent plastic strains, respectively, σ_{c0} is the initial compressive yield stress and σ_{cu} is the ultimate compressive stress [31].

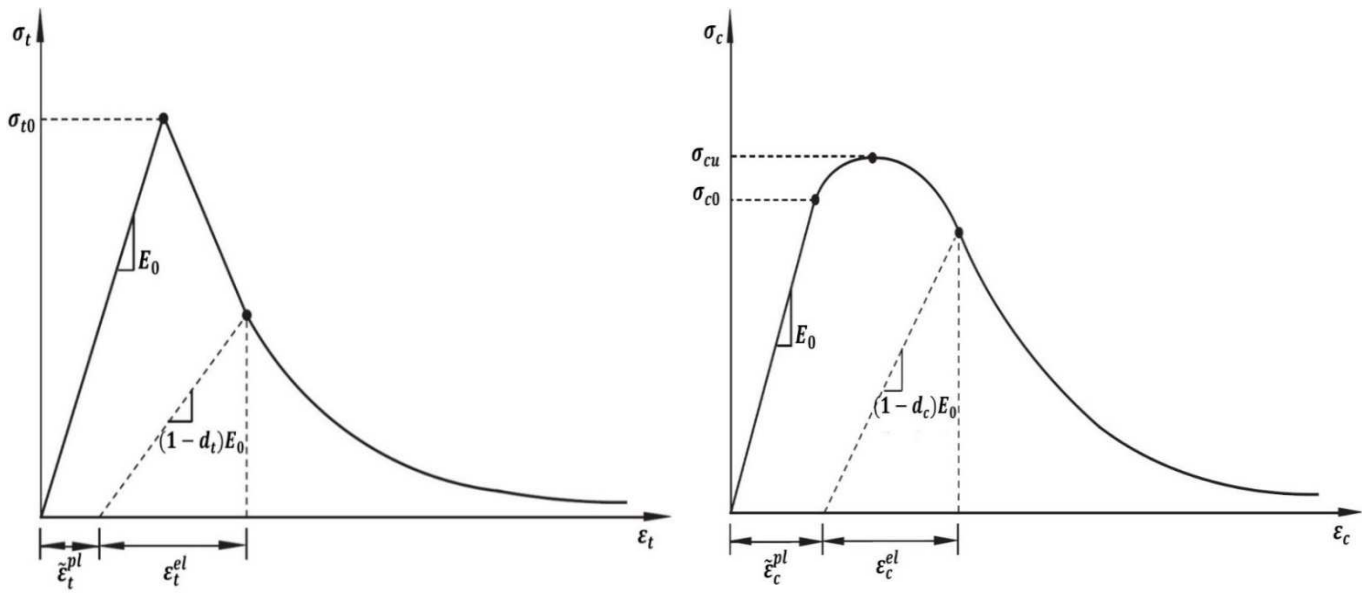

(a) (b)

Fig.4 Response of concrete to uniaxial loading in (a) tension and (b) compression [31]

Introduced parameter in CDP model of ABAQUS for concrete in tension and compression are presented in Table 2. The simulated stress-strain curves for concrete in tensile and compression, based on the CDP model, are illustrated in Figs. 5(a)-(b).

Table 2 Introduced parameter in CDF model of ABAQUS for concrete in tension and compression

Compression behavior			
stress	Crushing strain	d_c	Crushing strain
12.9827	0	0	0
13.4969	0.000003	0.001004818	0.000003
15.0916	0.000021	0.006300654	0.000021
16.588	0.000044	0.012967834	0.000044
17.9978	0.000071	0.021040948	0.000071
26	0.000658	0.193212546	0.000658
21.9844	0.001366	0.398104565	0.001366
12.948	0.002332	0.673582389	0.002332
10.6542	0.002550	0.735171214	0.002550
5.616	0.003010	0.864048294	0.003010
Tension behavior			
stress	Cracking strain	d_t	Cracking strain
2.49	0	0	0
1.75	0.00005	0.11	0.00005
0.75	0.00020	0.381	0.00020
0.01	0.00100	0.95	0.00100

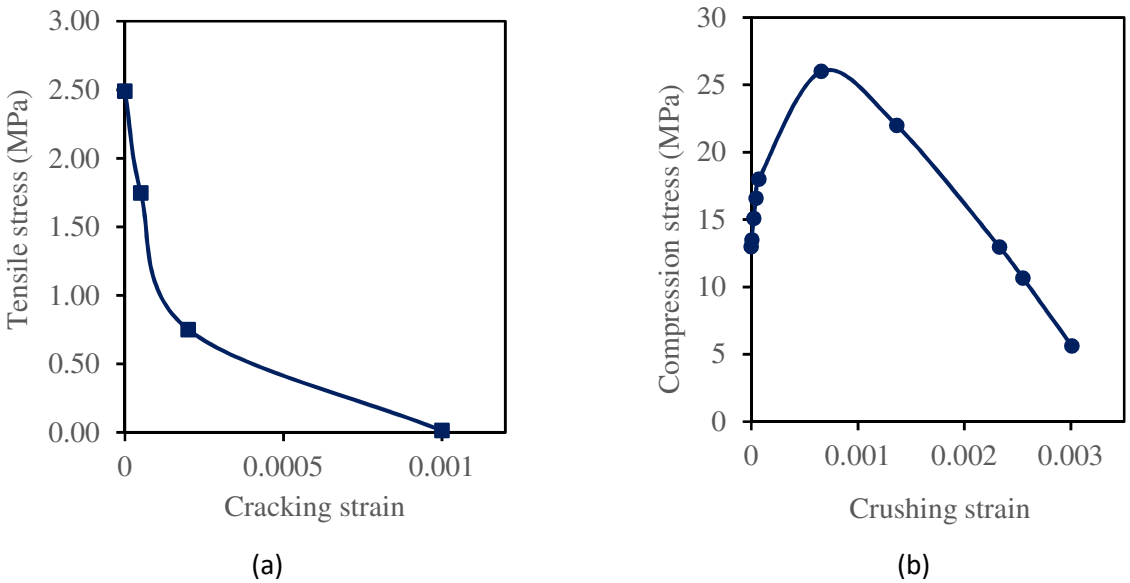

Fig. 5 Concrete stress–strain curve used for: (a) tension after cracking and (b) compression in CDP model

For cyclic analysis and pushover analysis of the models, kinematic hardening and isotropic hardening were used for the steel materials respectively. The modules of elasticity of steel is 200000 MPa. The

remaining material properties of used steels in the experimental test and FE simulation are shown in Table 3.

Table 3 Material properties of the used steel in experimental test and FE models

Steel			Yield strength (MPa)	Ultimate strength (MPa)
Column longitudinal reinforcement	Diameter (mm)	25	443	590
Column longitudinal reinforcement		22	430	590
Beam longitudinal reinforcement		16	471	590
Transverse reinforcement		10	486	590
Stud		13	240	370
Steel plate of connections (End plate)	Thickness (mm)	12	240	370
Steel plate of connections (Fish plate)		6	240	370
Infilled steel plate (SPSW)		2	302	440

The stress-strain curve of steel was taken as for an elasto-plastic material with linear strain hardening, see Fig. 6. The tangent modulus (E') in the plastic regime was set equal to 1% of initial modulus of elasticity (E).

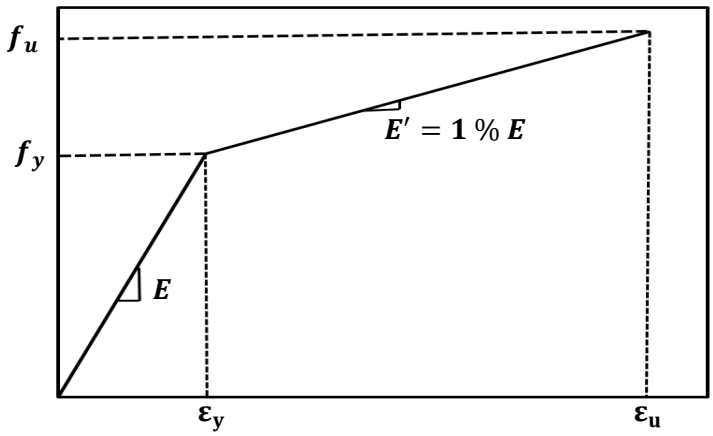

Fig. 6 Stress-strain curves for steel in finite element simulation (Elasto-plastic material with linear strain hardening)

2.4 Comparison FE analysis results with experimental data

Fig. 7 shows load-story drift ratio curve for 3D FE simulation and experimental test for both cyclic and pushover analysis. The load-story drift ratio curve of the 3D FE analyses indicate good agreement, for the ultimate limit state (ULS), with experimental observations. Figs. 8 (a)-(b) shows the deformation and

crack pattern of concrete in experimental specimen and the maximum plastic strains of concrete in FE model at ultimate displacement. As shown in this figures, the direction of cracks are perpendicular to the directions of plastic strains and cracked zones of concrete in experimental specimen and FE model are in an acceptable agreement. As shown in Fig. 8(c), evaluation of von Mises stress in FE model shows that SPSW is yielded at all the stories.

در شکلهای 8(d)-(e) به ترتیب خرابی کششی و فشاری بتن نشان داده شده است. مقایسه این شکلها با تغییرشکل نهایی بتن نمونه آزمایشگاهی (شکل 8(a)) انطباق قابل قبولی را نشان می دهد.

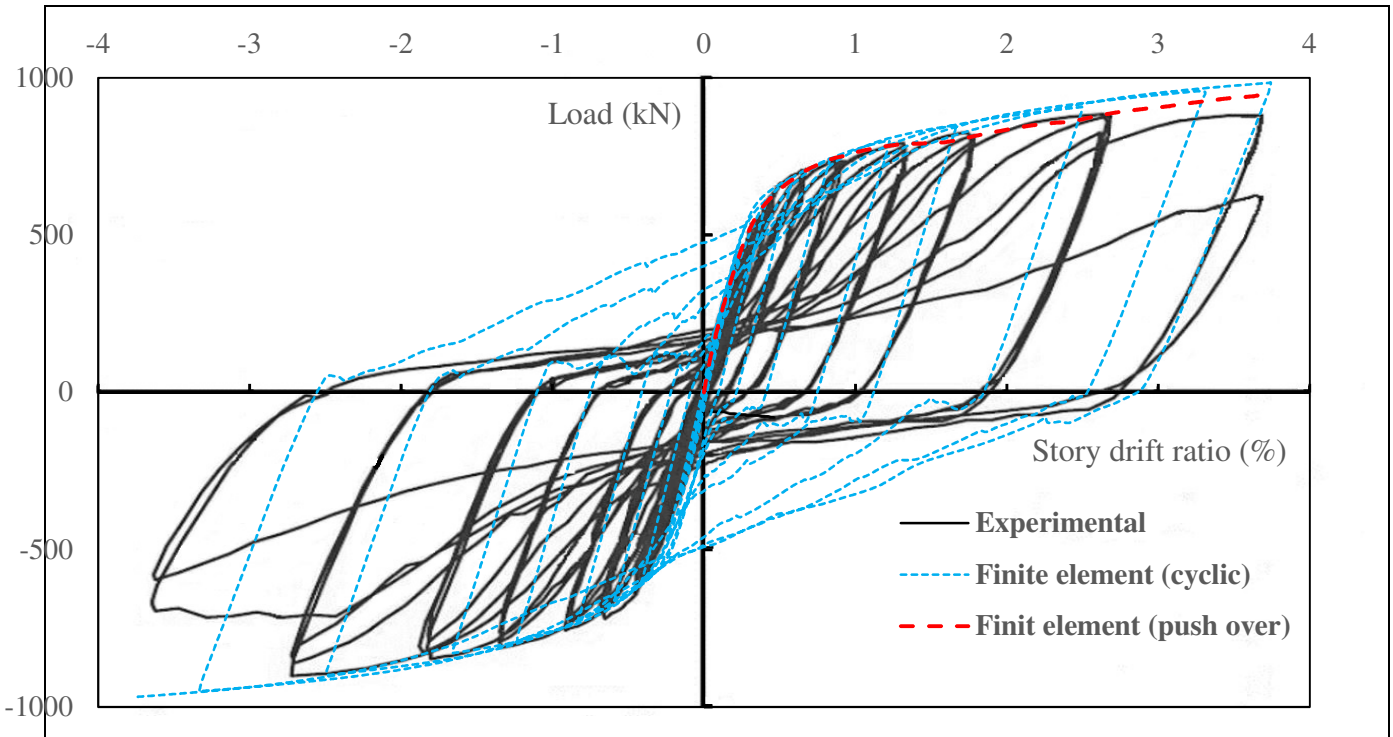

Fig. 7 Load- Story drift ratio curve for 3D FE simulation and experimental test (cyclic and push over analyze)

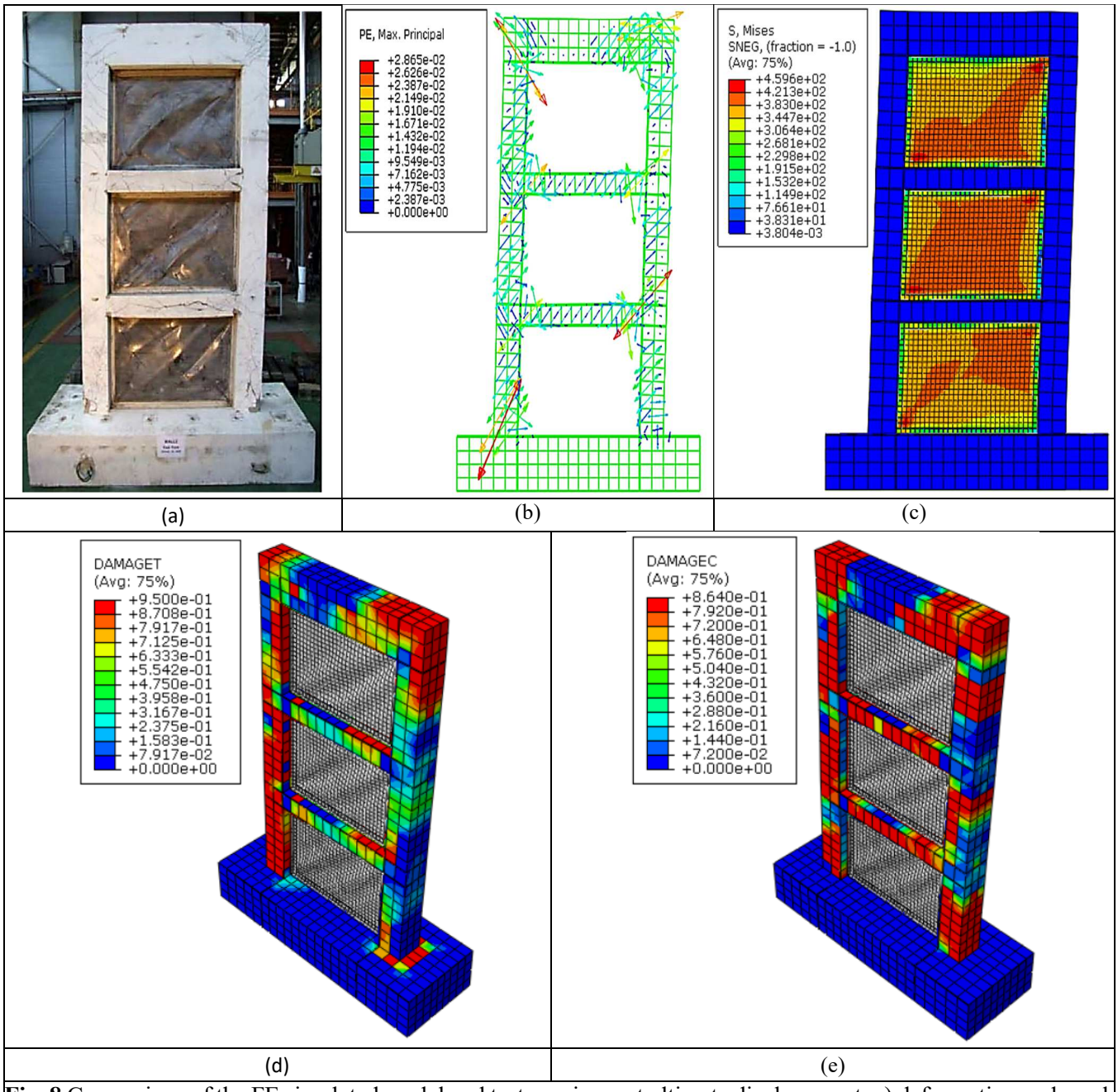

Fig. 8 Comparison of the FE simulated model and test specimen at ultimate displacement: a) deformation and crack pattern of experimental RCF in SPIW1 specimen, b) maximum plastic strains of concrete in the simulated model and c) von Mises stress distribution, d) concrete damage in tension, e) concrete damage in compresion

3. Proposed connections

In this paper, the performance of four types of proposed connection to transfer the tension field forces from SPSW to RCF are investigated. Three of these connection types are used for rehabilitation of RC structures and one is used for new construction. For comparability of results, material properties, meshing, boundary conditions and studs diameter of all models are considered to be the same as those of the

experimental specimen. The details of all connections are shown in Table 4 and Fig. 9. In all specimens, steel frame with plates (thickness = 12 mm and width = 300 mm) are used inside of the RCF, and SPSW is connected by L-section frame.

Table 4 Details of proposed connections (mm)

Connection			**U-shaped fish plate of columns**		**Continue plates of beams**	**Fish plate of beams**		**L-section frame**	**Inside frame**	
Type		Name	thickness	width	thickness	thickness	width		thickness	width
1	CC	CC-12-4-50	12	100	4	-	-	$50 \times 50 \times 5$	12	300
		CC-12-12-50	12	100	12	-	-	$50 \times 50 \times 5$	12	300
		CC-12-20-50	12	100	20	-	-	$50 \times 50 \times 5$	12	300
		CC-12-12-75	12	100	12	-	-	$75 \times 75 \times 6$	12	300
		CC-12-12-100	12	100	12	-	-	$100 \times 100 \times 10$	12	300
	CF	CF-12-6.56-50	12	100	-	6.56	100	$50 \times 50 \times 5$	12	300
		CF-12-20-50	12	100	-	20	100	$50 \times 50 \times 5$	12	300
		CF-12-32.8-50	12	100	-	32.8	100	$50 \times 50 \times 5$	12	300
2	CS	CS-12-12-50	12	100	-	-	-	$50 \times 50 \times 5$	12	300
		CS-6-6-50	6	100	-	-	-	$50 \times 50 \times 5$	6	300
		CS-6-6-75	6	100	-	-	-	$75 \times 75 \times 6$	6	300
		CS-6-6-100	6	100	-	-	-	$100 \times 100 \times 10$	6	300
			Fish plate of columns			L-sections used in corners of columns				
			thickness	width						
3	CSL	CSL-12-12-50	12	100	-	$50 \times 50 \times 5$		$50 \times 50 \times 5$	12	300
	CSSL	CSSL-12-12-50	12	100	-	$50 \times 50 \times 5$		$50 \times 50 \times 5$	12	300
			interval between connection stirrups			Yielding stress of connection stirrups				
			in the beams		in the columns					
4	S	S-60-50-486	60		50	486		$50 \times 50 \times 5$	12	300
		S-120-100-486	120		100	486		$50 \times 50 \times 5$	12	300
		S60-50-300	60		50	300		$50 \times 50 \times 5$	12	300

3.1. Type 1, CC and CF connections

In the type 1 connections, CC and CF connections that are shown in Figs. 9 (a)-(b) and Table 4, continuity plates and fish plates are respectively used in the beams instead of the studs. The parameters investigated in these connections are the connection plate thickness and the size of L-section frame connected to SPSW. To name CC and CF connection specimens, CC-t-t-L and CF-t-t-L styles are used respectively. The first letter on the left, C, represents the type of connection confined by plates. The second letter, C and F, represents the continuity plate and the fish plate in beams respectively. The other letters from left to right represents the column fish plate thickness, the connection plate thickness of beams and the size of L-sections connected to SPSW respectively. In this type of connection, eight specimens are investigated.

Connection plates of beams in the specimens with the CC connection are plates with thickness of 4, 12 and 20 mm. In the CF connection specimens, fish plates with equivalent thickness of 6.56, 20, 32.8 mm and width of 100 mm are modeled. In the both CC and CF connections, U-shaped fish plate (thickness = 12 mm, width = 100 mm) are used in the columns. In the L-section frame connected to SPSW, symmetric L-sections with sizes of 50×5, 75×6 and 100×10 mm are used. In the other words, ratios of the L-section thickness to the SPSW thickness (t_l/t_p), are respectively 2.5, 3 and 5.

3.2. Type 2, CS connections

In the type 2 connections, CS connection as shown in Fig. 9(c) and Table 4, two rows of studs embedded in the beams are used (diameter = 13 mm, length = 200 mm) at intervals of 130 mm. U-shaped fish plates (thickness = 12 mm, width = 100 mm) are used in the columns. Parameters investigated in this type of connection are the size of L-sections frame connected to SPSW and the thickness of inside frame. In the CS connection specimens, the plates of inside frame and the fish plates of the columns are modeled with two thicknesses of 12 and 6 mm. The specimens with 6 mm connection plates are, modeled by 50×5, 75×6 and 100×10 mm L-sections, In other words, the ratios of (t_l/t_p) are 2.5, 3 and 5 respectively. The CS connection specimens are named as CS-t-t-L, where the first letter from the left, C represents the type of connection confined by plates in the columns and S represents the located studs in the beams. The other letters from left to right, represent the columns fish plate thickness, the thickness of inside frame and the size of L-sections connected to SPSW respectively. In this type of connection, four specimens are investigated.

3.3. Type 3, CSL and CSSL connections

In Figs. 11(d)-(e), CSL and CSSL connections of type 3 are shown. This connection type are similar to the connection of type 2 with the difference of using of the L-section profiles at corners of the columns. In this type of connection, two specimens are investigated. Parameters investigated in this type of

connection are the presence of the L-section profiles at the columns corners and adding studs in the columns. As shown in Fig. 11(e) in CSSL connection, one row of studs (diameter = 13 mm, length = 310 mm), is placed in the columns. For naming these connection specimens, CSL-t-t-L and CSSL-t-t-L styles are used, where the C letter, similar to the previous type of connections, represents the type of connection confined by plates, and the first S represents the existence of studs in the beams and the second S represents the existence of studs in the columns. The other letters from left to right are similar to type 2 connection.

3.4. Type 4, S connections

In the type 4, as shown in Fig. 9(f), the inside frame is connected to RCF by embedded stirrups in the beams and the columns. As shown in Fig. 11(g), the stirrups of connections are located through the beams and columns stirrups. The parameters investigated in this type of connection are yielding stress and distance of stirrups of connections. For naming the S connection specimens, S-x-y-f style is used, where the S letter represents the type of connection, additional stirrups connection. The other letters from left to right represent the interval between the connection stirrups in beams and columns and the yielding stress of connections stirrups respectively. In this type of connection, three specimens are investigated.

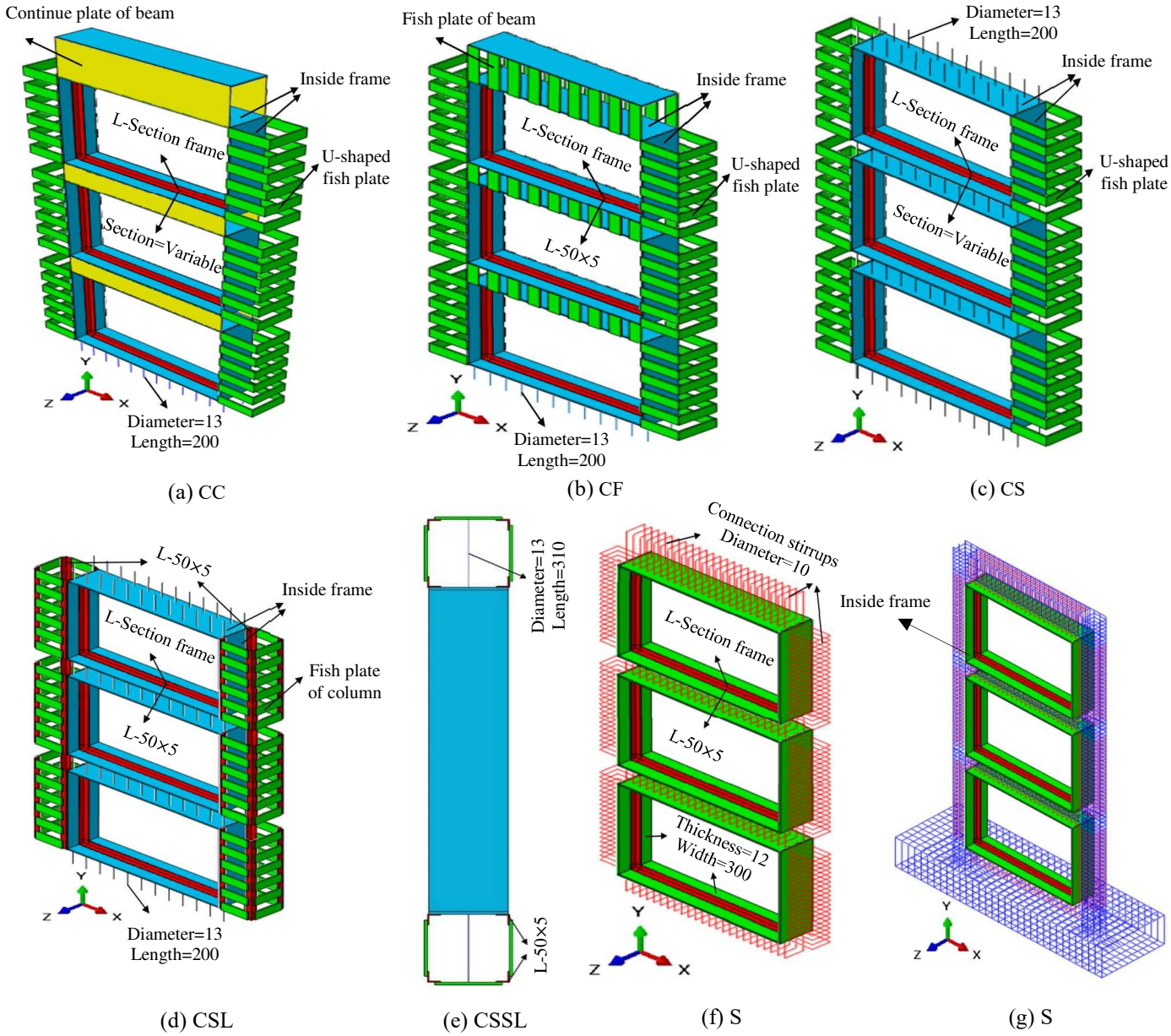

Fig. 9 Details of the different types of connections, (a) and (b) are type 1, (c) is type 2, (d) and (e) are type 3 and (f) and (g) are type 4, dimensions are in mm.

4. Results and discussion

4.1. Failure mechanism and behavior of models

Steel Plate Shear Walls

The selected constitutive material law to represent steel behavior is the von Mises yield criterion. Fig. 10 shows the von Mises stress distribution in SPSW for some of the investigated

models at ultimate displacement level. Since similar performance is observed for the other specimens, only some of the results are presented herein. The yielding stress of SPSW material is 302 MPa.

In Fig. 10(a), the von Mises stress in SPSW with type 1 connection of CC-12-4-50 model is shown. As can be seen in this Figure, the distribution of yield zones in SPSW is not uniform along the wall height and it is concentrated in the tension diagonal zone. Yield zones of SPSW in the other specimens of CC and CF connections (type 1), where 50×5 mm L-section frame is used to connecting SPSW, are similar to this specimen. Von Mises stresses in SPSW of CC-12-12-75 and CC-12-12-100 models are shown in Figs. 10(b)-(c) respectively. In CC-12-12-100 model where 100×10 mm L-section are used, distribution of the yield stress in SPSW along the wall height is more extensive than that of the specimens where 50×5 and 75×6 mm L-sections frames are used. It means that by increasing the size of the L-section, the capacity of SPSW is used effectively. The reason for desirable distribution of yielding in SPSW can be attributed to adequate rigidity of the L-section frames connected to SPSW.

Fig. 10(d) shows the von Mises stress in SPSW with type 2 connection of CS-12-12-50 model. In this connection type, the yield stress distribution in SPSW along the wall height is broader than the type 1 connections with the same properties. Consequently, it can be concluded that the studs embedded in the beams instead of connection plates caused better transfer of tension field force of SPSW to RCF. The von Mises stress in SPSW of CS-6-6-100 model is shown in Fig. 10(e). Comparing the distributions of yield stress in Figs. 10(d)-(e) shows more extensive yield zone in CS-6-6-100 model than CS-12-12-50 model which implies efficient performance of CS-6-6-100 connection.

The von Mises stress in SPSW with type 3 connection of CSL-12-12-50 model is shown in Fig. 10(f). The yield stress is distributed more extensive than that in the specimens with Type 1 connections with similar properties, i.e. CC and CF. However, similar to CS connection

specimens with similar properties (type 2), distribution of yielding in SPSW is not uniform along the wall height. This demonstrates that, with the same connection properties, the use of the L-section profiles in column corners has no significant effect on uniform distribution of yield stress in the height of SPSW. In Fig. 10(g), the von Mises stress in SPSW of CSSL-12-12-50 model is shown. The results demonstrate the effect of using studs in the columns. As it is indicated in the figure, yield stress in SPSW is uniformly distributed along the wall height. In this specimen, yield zones of SPSW are more extensive than those in CSL-12-12-50 specimen. The use of studs in the beams as well as in the columns to connect SPSW to RCF, has demonstrated desirable performance.

In Fig. 10(h) von Mises stress in SPSW with type 4 of S-60-50-486 model is shown. According to this figure, yield stress of SPSW is uniformly distributed in the height of the wall. Compared to the other types of connections this type of connection demonstrates better behavior in term of transferring the tension stress of SPSW to the RCF.

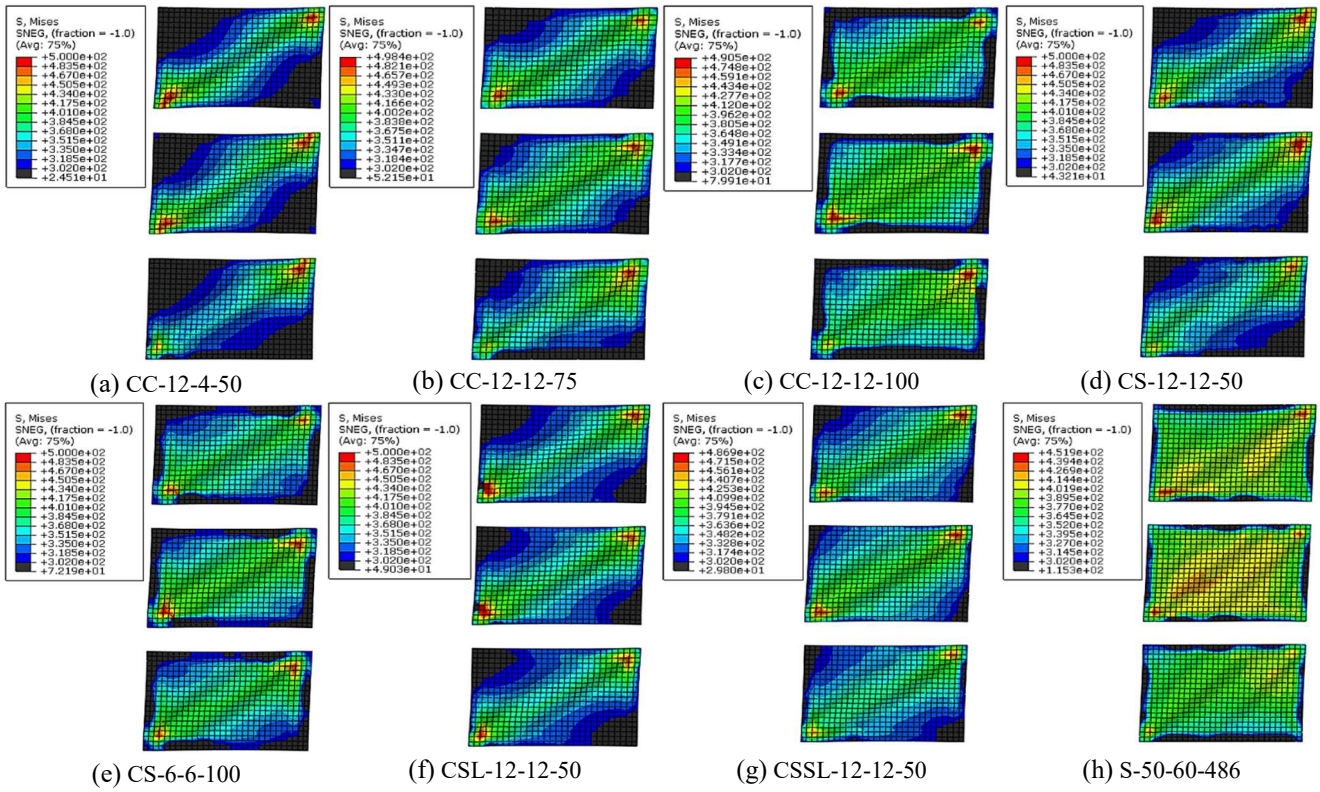

(a) CC-12-4-50 (b) CC-12-12-75 (c) CC-12-12-100 (d) CS-12-12-50

(e) CS-6-6-100 (f) CSL-12-12-50 (g) CSSL-12-12-50 (h) S-50-60-486

Fig. 10 Von Mises stress in SPSW of the investigated models at ultimate displacement, (a)-(c) are type 1, (d) and (e) are type 2, (f) and (g) are type 3 and (h) is type 4. For details of different types of connection, see Table 4.

Connections

The von Mises stress distribution in connections at ultimate displacement has been shown in Fig. 11. Since the other specimens showed similar performance, only some of the results are presented herein. Fig. 11(a) shows the von Mises stress in the experimental specimen connection, SPIW1. Observation of the yield stress distribution in the connection plates and studs shows that the connection plates are yielded only in the edge of spans and have lower stresses in the middle areas of the span. According to the obtained results, none of the studs embedded in the foundation, first and second stories are yielded. In Figs. 11(b)-(c) the von Mises stresses in the selected models of type 1, CC-12-4-50 and CF-12-6.56-50 models, are shown. As shown in the Figures, the L-section frame connected to SPSW is only yielded in the edge zones of span where the lower stresses are obtained in the mid span. It is observed that, none of the fish plates connected to the columns and the studs embedded in the foundation are yielded.

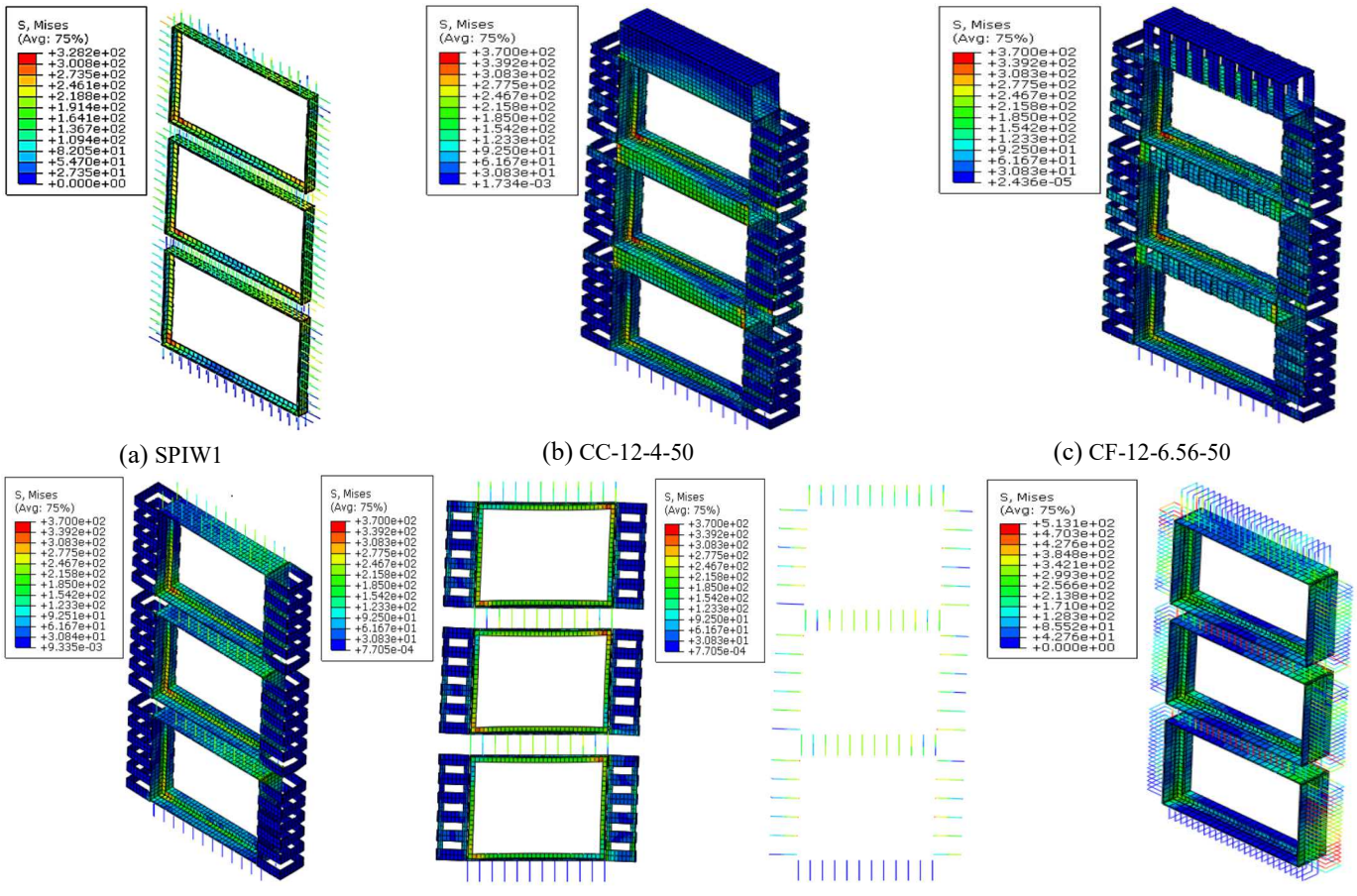

(a) SPIW1 (b) CC-12-4-50 (c) CF-12-6.56-50

(d) CS-12-12-50 (e) CSSL-12-12-50 (f) CSSL-12-12-50 (g) S-60-50-486

Fig. 11 Von Mises stress in connections of the investigated models at ultimate displacement: (a) experimental specimen, SPIW1, (b) and (c) are type 1, (d) is type 2, (e) and (f) are type 3 and (g) is type 4. For details of different types of connection, see Table 4.

In Fig. 11(d) the von Mises stress distribution in the model CS-12-12-50 of type 2 connections is shown. Yielded zones of the L-section frames and the connection plates are similar to those in the specimens CC and CF of connections type 1. Except the studs embedded in the foundation, the studs of the first, second and third stories are yielded. In Figs. 11(e)-(f), the von Mises stress in the model CSSL-12-12-50 of type 3 connections is shown. Yielded zones of the L-section frames and the connection plates are similar to the previous connections. The L-section profiles in the corners of the columns are not yielded. Except for the studs embedded in the foundation, studs of the beams and columns in all stories are yielded, see Fig. 11(f). Fig. 11(g) shows the von Mises stress distribution in the model S-60-50-486 of type 4 connections. Yielded zones of the L-section frames and the connection plates are similar to those in other types of connection specimens. Except for the connection stirrups embedded in the foundation and the third story beam, stirrups of the beams and columns in all stories are yielded.

4.2. Load-displacement relationships of the connections

Type 1, CC and CF connections

Fig. 12 compares the load-displacement curves obtained from the analysis of type 1 connections. According to this figure, strength of the specimens with 50×5 mm L-section frame $((t_l/t_p) = 2.5)$, is lower than that of the experimental specimen (SPIW1). As it discussed in part 4.1, in failure mechanism of this type of connection, the yield stress distribution in SPSW is not uniform along the wall height, see Fig. 10(a). As regards in this type of connection, studs are not used in the beams and columns; therefore, the connection plates that placed out of concrete do not have enough connection with concrete as in the case of using studs. Since a specific connecting method is more preferable for existing condition, in the case of RCF structures rehabilitation, the use of this type of connection for structures with lack of resistance in the boundary frame is recommended. To improve the performance of this

type of connection, parameters including the thickness of the connection plates of beams and the size of the L-section frames connected to SPSW are investigated. The results shows that using of the connection plates of beams with 3 to 5 times more than the original thickness does not significantly increase the strength of specimens. Thus, excessive increase of the thickness of connection plates of beams will result in uneconomic connections. Therefore, for improving the connection performance, the L-section frames with size of 75×6 mm, $(t_l/t_p) = 3$, and 100×10 mm, $(t_l/t_p) = 5$, are used to connect SPSW. As shown in the results, in model with ratio of $(t_l/t_p) = 5$, the maximum strength of specimen is higher than that of the experimental specimen (SPIW1). This result can be justified by the failure mechanism of SPSW in this specimen. As it was mentioned earlier, by increasing the size of the L-sections, uniform yielding distribution along the height of SPSW are observed, see Figs. 10(b)-(c). This is show that in order to not using studs in SPSW connection, the members connected to SPSW must have sufficient stiffness. Otherwise, because of the large deformation of boundary members, tension field forces of SPSW decreases and is not well transferred from the wall to the RC frame. It can be concluded that instead of increasing the thickness of beam connection plates that induce uneconomic connections, increasing the size of the L-sections frame connected to SPSW is more effective to increase the strength.

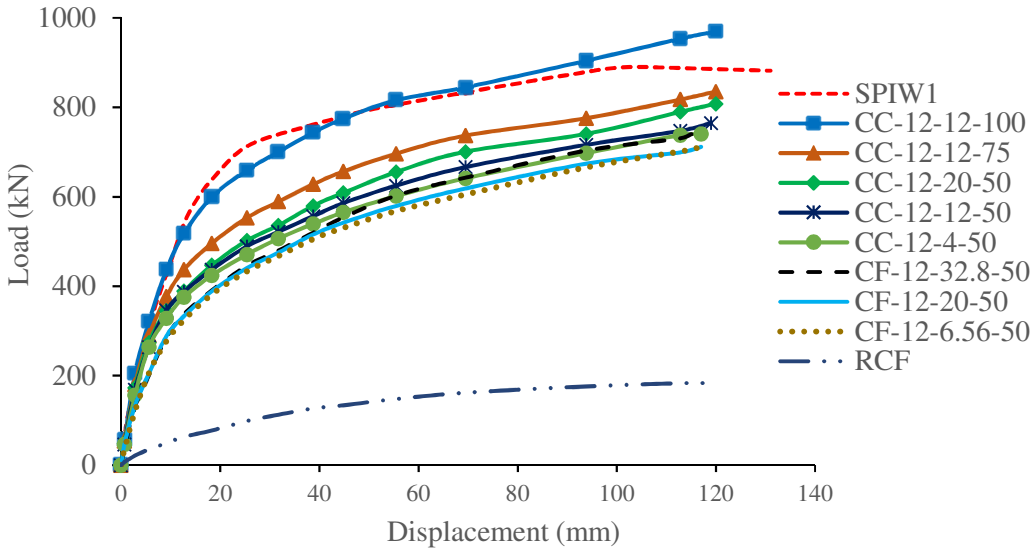

Fig. 12 Comparison of load-displacement curves of experimental specimen (SPIW1) and models with type 2 connections

Type 2, CS connections

A comparison between the load-displacement relationships obtained from the analysis of models with CS connection is shown in Fig. 13. As shown in the figure, in the CS-12-12-50 specimen where (t_l/t_p) ratio is 2.5, the maximum strength of specimen is less than that of the experimental specimen (SPIW1). In CS-6-6-50 specimen, where the thickness of steel plate connection (inside frame) is 6 mm and the ratio of $(t_l/t_p) = 2.5$, the minimum load carrying capacity is obtained. Load-displacement curves of CS-12-12-50 and CS-6-6-75 models are coincident. The volume of steel plates used in the connection plates and the L-section frames for CS-6-6-75 specimen is reduced by 41% compared to the CS-12-12-50 specimen. However, the increase of the size of L-section frame compensates the reduction of the load carrying capacity.

Load-displacement curve of CS-6-6-100 is higher than that of the experimental specimen (SPIW1). The volume of steel plates used in the connection plates and the L-section frames of CS-6-6-100 specimen is reduced by 25% compared to CS-12-12-50 specimen. This result shows that increasing in the size of L-section frames compensates the reduced load carrying

capacity and this specimen showed better performance than the CS-12-12-50 specimen. Therefore, increasing the connection plate thickness has lower effect on increasing the load carrying capacity than the L-section frame size.

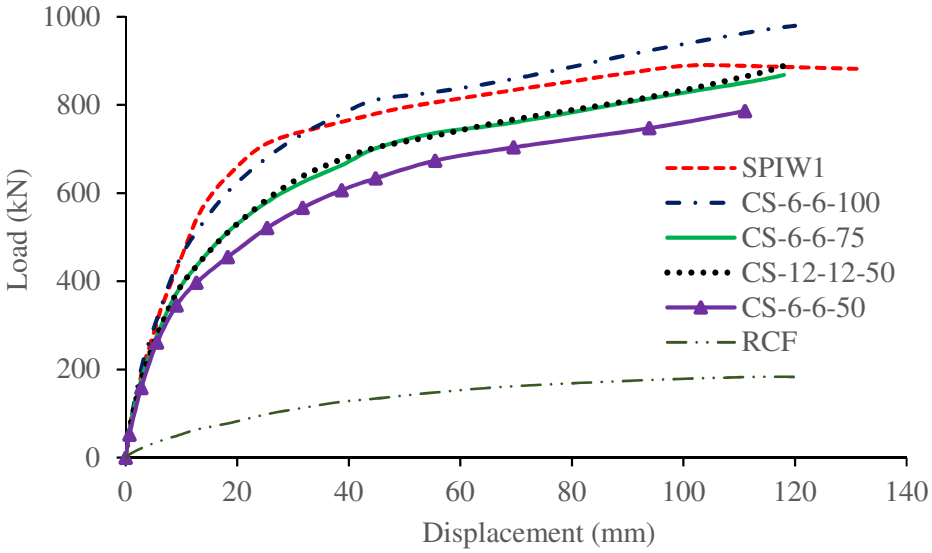

Fig. 13 Comparison of load-displacement curves of experimental specimen (SPIW1) and models CS in type 2 connections

Type 3, CSL and CSSL connections

Fig. 14 compares the load-displacement curves obtained by the analysis of models with CSL and CSSL connections. In CSL-12-12-50 specimen where two rows of studs are embedded in the beams, lower strength is obtained compared to CSSL-12-12-50 specimen, where one row of studs is embedded in the columns in addition to the studs in the beams. Maximum load carrying capacity of CSSL-12-12-50 specimen is more than that of the experimental specimen (SPIW1). This result shows providing the L-section profiles at the corners of the columns has little effect on increasing of the system strength.

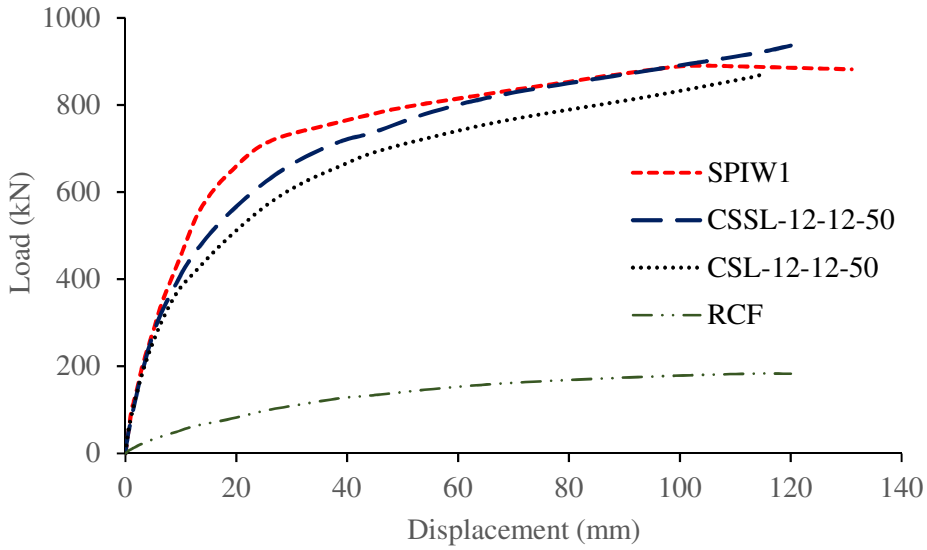

Fig. 14 Comparison of load-displacement curves of experimental specimen (SPIW1) and models CSSL and CSL in type 3 connections

Type 4, S connections

Fig. 15 illustrates the load-displacement behaviors obtained by analysis of models with S connections (connection type 4). Comparison between load-displacement curves of S-60-50-486 and S-120-100-486 specimens shows that the linear parts of the curves are coincident and in the nonlinear part, doubling interval of additional stirrups connection in S-120-100-486 specimen cause 10% reduction of maximum strength. Comparing the load-displacement curves of S-60-50-486 and S-60-50-300 specimens, shows that the linear part of the curves are the same and after the displacement of 100 mm, the use of connection stirrups with lower yield stress (S-60-50-300) results in drop of the maximum strength of specimen by 3 %.

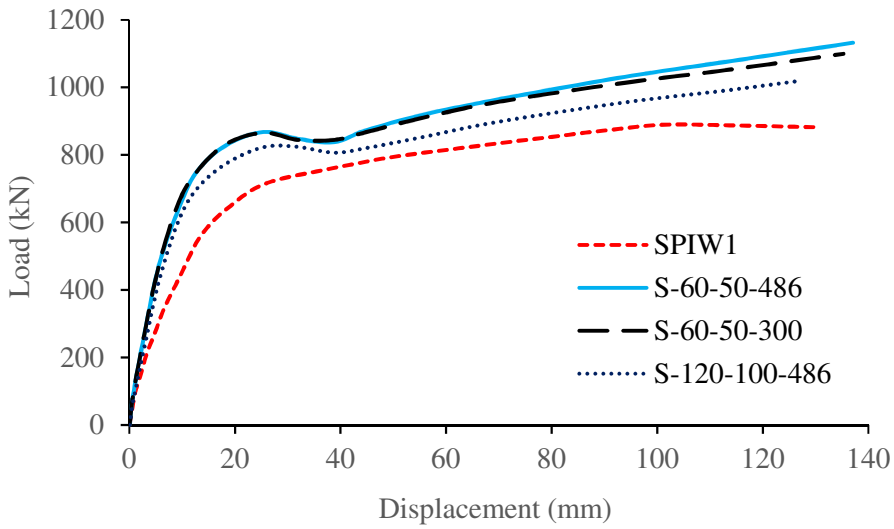

Fig. 15 Comparison of load-displacement curves of experimental specimen (SPIW1) and models S in type 4 connections

4.2.Comparison of connection behavior

Fig. 16 compares the load-displacement curves of models with all types of the connections. To avoid swarm of the curves, some models from CC, CF and CS connections are selected. As shown in the figure, S-60-50-486 specimen, from type 4 connections, has the maximum load carrying capacity. The connections used for the experimental specimen (SPIW1) and S connection (Type 4) is applicable for new constructions. The results of load carrying capacity of the specimens show that S connection has more appropriate performance compared to the experimental specimen and other specimens. S connection, can be used as an appropriate method to connect SPSW to RCF. From those specimens of the three connection types that are applicable for rehabilitation, CS-6-6-100 specimen (type 2) has the maximum strength and after that, CC-12-12-100 (type 1) and CSSL-12-12-50 (type 3) specimens have the maximum strength respectively. Since in CSSL-12-12-50 specimen, the studs are placed in the beams and columns and the L-section profiles are placed in the corners of columns, the strength of this specimen is lower than CS-6-6-100 specimen (where the studs are used only in the beams and thickness of connection plates is 6 mm) and CC-12-12-100 specimen (where the studs are not

used in the beams and columns). However, the volume of all connection plates used in CSSL-12-12-50 specimen is increased by 40% compared to that in CS-6-6-100 specimen. This results demonstrate that in the connections type 3, CSL and CSSL specimens, placing the L-section profiles at the corners of the columns will not significantly affect the strength capacities compared to CS connection specimens (type 2) with similar conditions. Increasing the size of L-sections connected to SPSW is more effective for increasing the strength.

Although the thickness of connection plates in CC and CF connection specimens are selected to be 12 mm, if the equal size of L-section frame is used, in the specimens of CS connection (where the thickness of connection plates is 6 mm), higher strength will be observed. CS-12-12-50 and CC-12-12-50 specimens have equal thickness of connection plates and size of L-section frame connected to SPSW, but the strength of CS-12-12-50 specimen is higher. This result can be justified by yielding mechanism of the specimens. The use of studs in the beams improves the connection performance.

Connections of the types 1-3, i.e. specimens CC, CF, CS, CSL and CSSL, are applicable for rehabilitation of RC structures; performance of this connections demonstrated that the use of CC and CS connections with the thickness ratio of L-section frame (connected to SPSW) to SPSW $(t_l/t_p) = 5$, are more desirable. Among these three types of connections, the use of CC and CS connections is preferable to CSL and CSSL connections. Between CC and CS connections by similar conditions, the use of CS connection is preferred. CS connection is the optimum connection method from the consumed steel volume point of view.

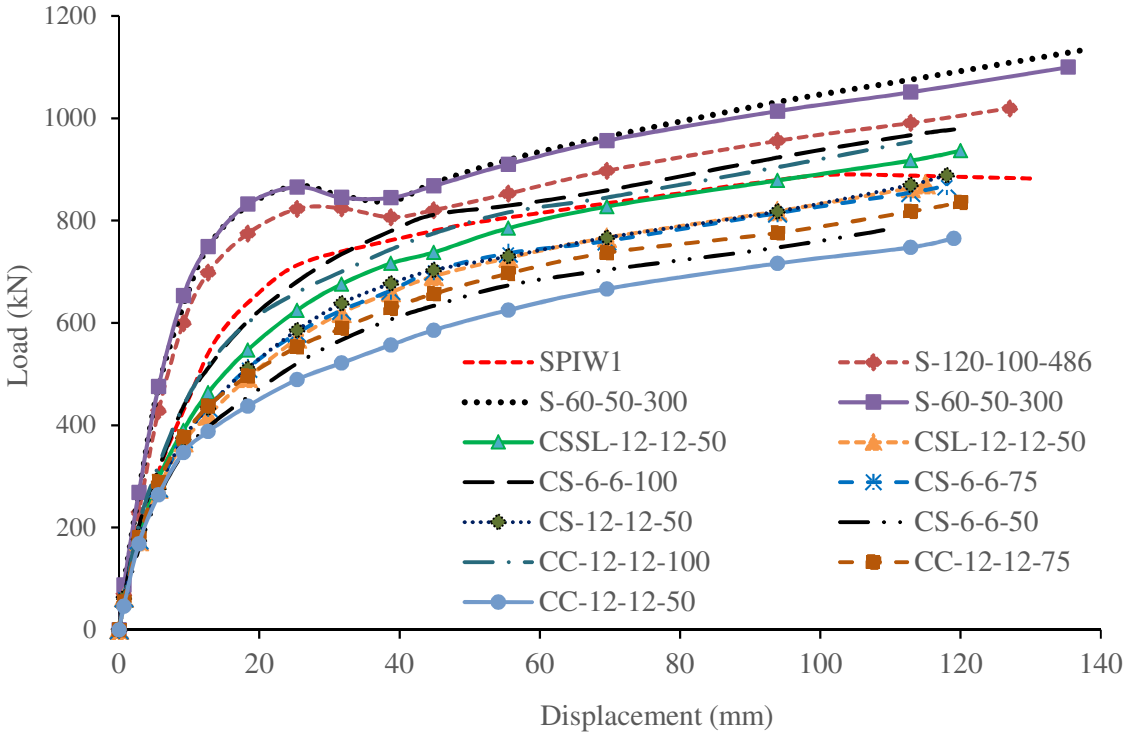

Fig. 16 Comparison of the load-displacement curves in all specimens

For further comparison of the results, the maximum load carrying capacities of all specimens are shown in Fig. 17. CS-12-12-50 and CS-6-6-50 specimens modeled to investigate the effect of connection plate (inside frame) thickness. The result demonstrate that by doubling the thickness of connection plates (inside frame), the maximum load carrying capacities increases by 13%. Average value of the maximum load carrying capacity for type 1 (CC), type 1 (CF), type 2 (CS), type 3 (CSL and CSSL) and type 4 (S) connection specimens are, 4.5, 3.95, 4.81, 4.94 and 5.92 times of the RCF load carrying capacity, respectively.

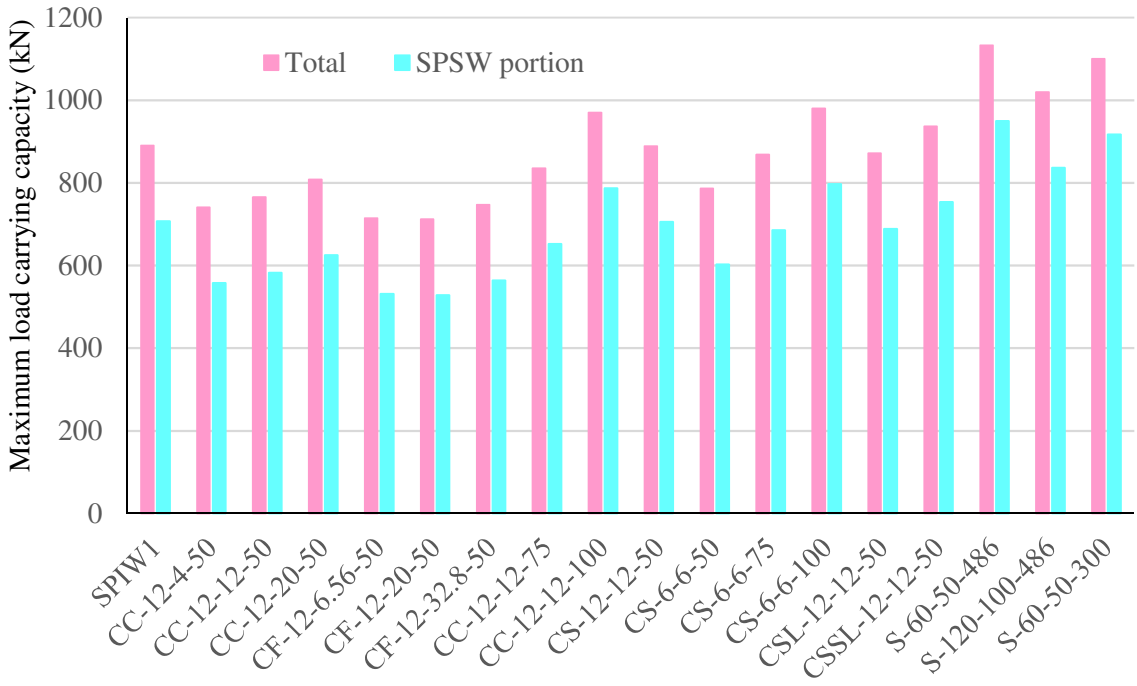

Fig. 17 Comparison of the maximum load carrying capacity and portion of SPSW along with connections in the maximum load carrying capacity in all specimens

4.3. Portion of SPSW load carrying capacity in the connections

When the load-displacement curve of RCF is obtained, portion of SPSW along with connections in the maximum load carrying capacity of all specimens can be separated from the total load-displacement curve. In Fig. 17, the portion of SPSW along with connections from the maximum load carrying capacity in all specimens are shown. The results show that in dual system of RCF and SPSW, on average, 78.6% of the maximum load carrying capacity is the portion of SPSW along with connections.

4.4. Behavior factor

In this paper, to calculate the behavior factor of the specimens, Uang [32] method is used as Eq. (2).

$$R = R_R.R_\mu.R_S \tag{2}$$

where R_R is redundancy factor and, due to the high redundancy of SPSW, is considered equal to 1, R_μ is ductility factor and R_S is overstrength factor. By simplifying the elastoplastic envelope curve using bilinear elastic-perfect plastic curve (Fig. 18), ductility of structures can be estimated by Eq. (3).

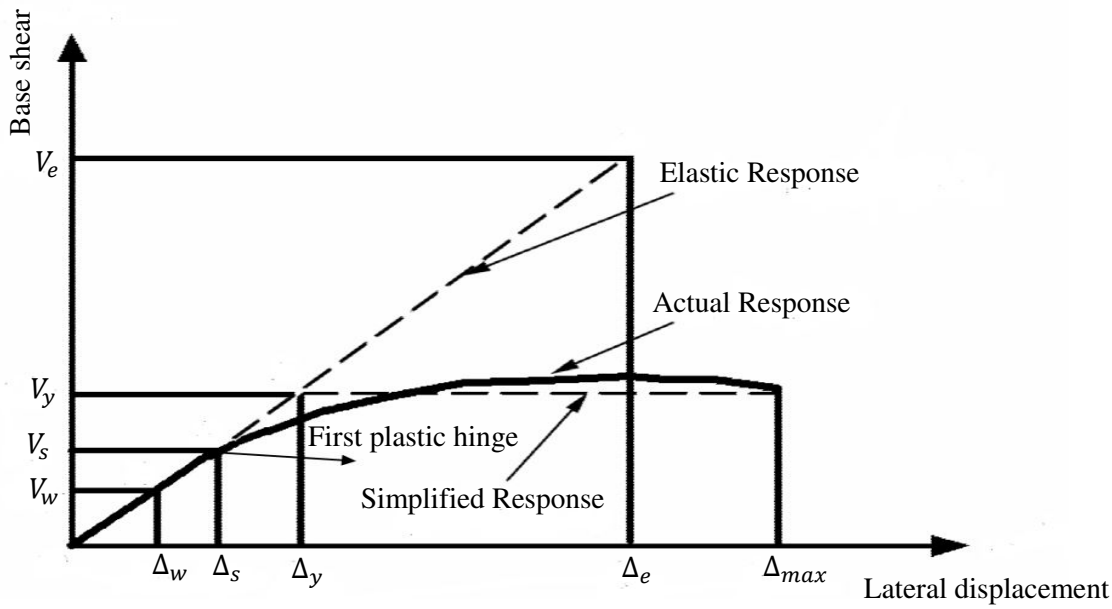

Fig. 18 Actual response (push over curve) and simplified response

$$\mu = \frac{\delta_{\max}}{\delta_y} \tag{3}$$

where, δ_{max} is the maximum lateral displacement and δ_y is yield displacement.

Structures can dissipate significant amount of earthquake energy with hysteretic behavior by means of ductility. Because of this energy dissipation capacity, elastic design strength (V_e) can be reduced to yield strength (V_y). According to this, the ductility reduction factor can be estimated by Eq. (4).

$$R_\mu = \frac{V_e}{V_y} \tag{4}$$

To estimate the ductility reduction factor, relationships have been proposed by different researchers [33-35]. In this investigation, the ductility reduction factor formulation proposed

by Newmark and Hall [33] is used. Newmark and Hall [33] proposed relationships to estimate the ductility reduction factor for elastic-perfect plastic single degree of freedom (SDOF) systems as Eq. (5)-(7). According to these equations, ductility reduction factor depends on period and ductility. Thus, frequency analysis is carried out for all specimens and period of specimens is estimated to be about 0.13 second.

The residual strength of structures after the formation of the first plastic hinge is called overstrength factor and can be estimated by Eq. (8). The values of behavior factor and overstrength factor for some structural systems in ASCE 7-10 [36] and NHERP [37] are listed in Table 5.

For frequencies above 33 Hz (periods below 0.03 second) $$R_\mu = 1 \quad (5)$$

For frequencies between 2 Hz and 8 Hz (periods between 0.12 second and 0.5 second) $$R_\mu = \sqrt{2\mu - 1} \quad \frac{\mu}{R_\mu} \geq 1 \quad (6)$$

For frequencies less than 1 Hz (periods exceeding 1 second) $$R_\mu = \mu \quad (7)$$

$$R_S = \Omega_0 = \frac{V_y}{V_s} \quad (8)$$

Table 5 Values of behavior factor and overstrength factor according to ASCE 7-10 [36] and NHERP [37]

Codes	Type of structural system	Ω_0	R
ASCE 7-10 [36]	Special reinforced concrete frame	3	8
	Special reinforced concrete frame + Special reinforced concrete shear wall	2.5	7
	Special steel frame + Steel special plate shear wall	2.5	8
NHERP 2003 [37]	Special reinforced concrete frame	3	8
	Special reinforced concrete frame + Special reinforced concrete shear wall	2.5	8
	Special steel frame + Steel special plate shear wall	2.5	8

Ductility, behavior factor and overstrength factor of the specimens are shown in Table. 6. Fig. 19 shows a comparison between the ductility and behavior factors of all specimens. As it can be seen, connections type 4, S specimens, have the maximum ductility. Average value of ductility for type 1 (CC), type 1 (CF), type 2 (CS), type 3 (CSL and CSSL) and type 4 (S) connection specimens are 1.45, 1.07, 1.32, 1.32 and 1.77 times of the RCF ductility

respectively. The average value of ductility in type 2 (CS) and type 3 (CSL and CSSL) connections is the same.

Table 6 Ductility, behavior factor and overstrength factor calculated for all specimens

Specimens		$\delta_Y\ (mm)$	$\delta_{max}\ (mm)$	μ	$V_y\ (kN)$	$V_s\ (kN)$	Ω_0	R_μ	R
Experimental	RCF	29.90	209.10	6.99	160.92	75	2.14	3.60	7.73
	SPIW1	14.60	131.60	9.01	812.37	400	2.03	4.13	8.38
Type 1	CC-12-4-50	11.45	117.00	10.21	9.92	310	1.93	4.41	8.52
	CC-12-12-50	11.90	119.00	10.00	622.75	320	1.95	4.36	8.48
	CC-12-20-50	12.00	120.00	10.00	651.94	320	2.04	4.36	8.88
	CF-12-6.56-50	15.89	118.00	7.43	574.91	280	2.05	3.72	7.64
	CF-12-20-50	15.20	117.00	7.70	577.03	280	2.06	3.79	7.82
	CF-12-32.8-50	15.80	116.00	7.34	593.35	280	2.11	3.70	7.82
	CC-12-12-75	12.10	120.00	9.92	688.64	350	1.97	4.34	8.54
	CC-12-12-100	11.90	120.00	10.08	804.08	400	2.01	4.39	8.80
Type 2	CS-12-12-50	12.80	118.00	9.22	728.59	360	2.02	4.17	8.45
	CS-6-6-50	13.00	111.00	8.54	643.73	320	2.01	4.01	8.10
	CS-6-6-75	12.20	118.00	9.67	715.94	360	2.00	4.28	8.52
	CS-6-6-100	12.60	120.00	9.52	818.58	410	2.00	4.25	8.48
Type 3	CSL-12-12-50	12.20	115.00	9.43	711.86	340	2.90	4.23	8.85
	CSSL-12-12-50	13.20	120.00	9.09	778.80	370	2.10	4.14	8.72
Type 4	S-60-50-486	11.00	137.00	12.45	967.27	580	1.67	4.89	8.15
	S-120-100-486	10.50	127.00	12.09	886.63	500	1.77	4.81	8.54
	S-60-50-300	10.80	135.00	12.50	949.68	580	1.64	4.90	8.02

According to the results presented in Table 6, the average value of the behavior factor and the overstrength factor for dual system of special RCF with SPSW are estimated to be 8.37 and 2 respectively. As shown in Fig. 19, comparison of the behavior factors shows that CF connection in type 2 and S connection specimens in type 4 have the minimum behavior factor. The parameters that are used to estimate the behavior factor are ductility and overstrength factor. S connection specimens have the maximum ductility. The reason for reduction of the behavior factor is the lower overstrength factor in these specimens. This reduction can be attributed to the failure mechanism of these specimens. In S connection specimens, due to high stiffness, the first plastic hinge is formed by large forces and then the plastic hinges are transferred to the columns of the first story where failure occurs.

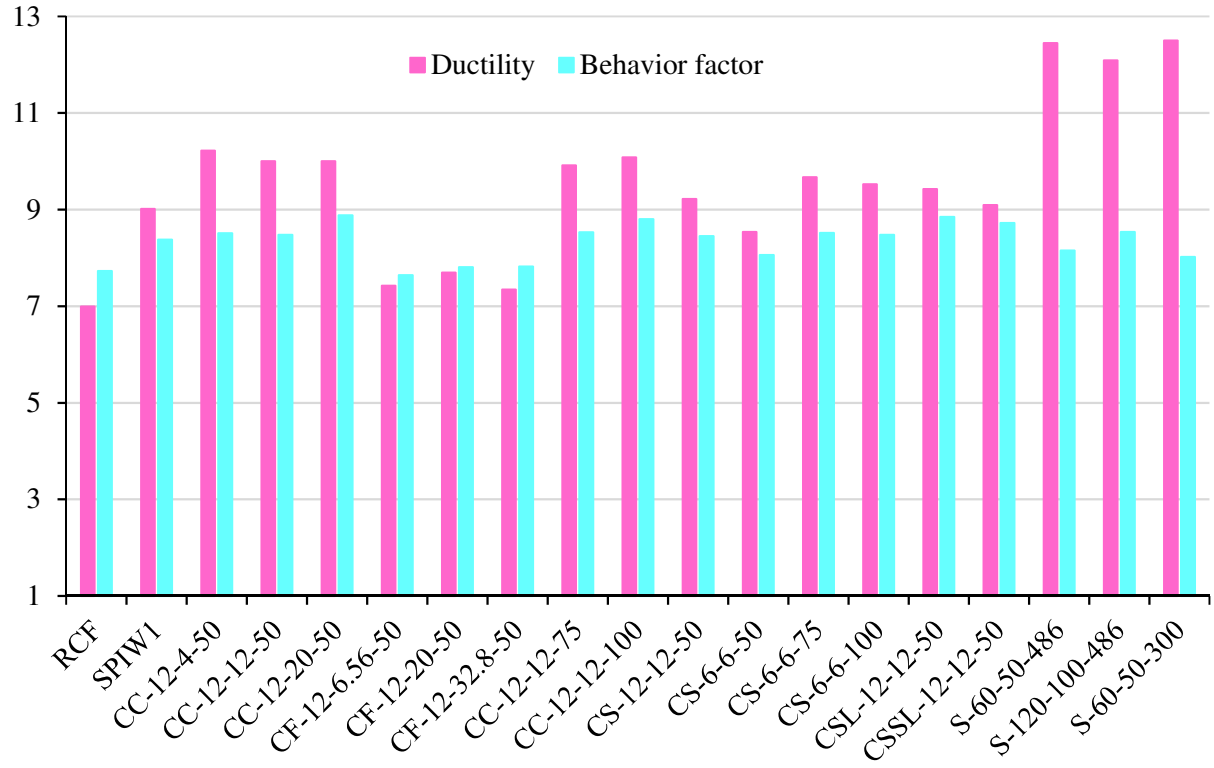

Fig. 19 Comparison of ductility and behavior factor in all specimens

4.5. Initial Stiffness

After the approximation of the load-displacement curve, initial stiffness of specimens can be estimated by Eq. 9 [28]. In Fig. 20 the initial stiffness of all specimens is shown. According to the results, S connection specimens have the maximum initial stiffness. The average value of initial stiffness for type 1 (CC), type 1 (CF), type 2 (CS), type 3 (CSL and CSSL) and type 4 (S) connection specimens are 10.54, 6.92, 10.69, 10.9 and 16.13 times of the initial RCF stiffness respectively. It can be seen that the CC (type 1), CS (type 2) and CSL (type 3) specimens have the same stiffness. By observing the stiffness of connections type 3, it can be see that placing L-sections in the corner of columns is not significantly increased the stiffness of the specimens. However, stiffness of connections type 2 is significantly increased by increasing the size of L-section frame connected to SPSW. According to obtained results, it

could be concluded that without using studs in the columns and beams, increasing the stiffness of the systems is possible (using the large size of L-section frame connected to SPSW).

$$K_y = \frac{V_y}{\delta_y} \tag{9}$$

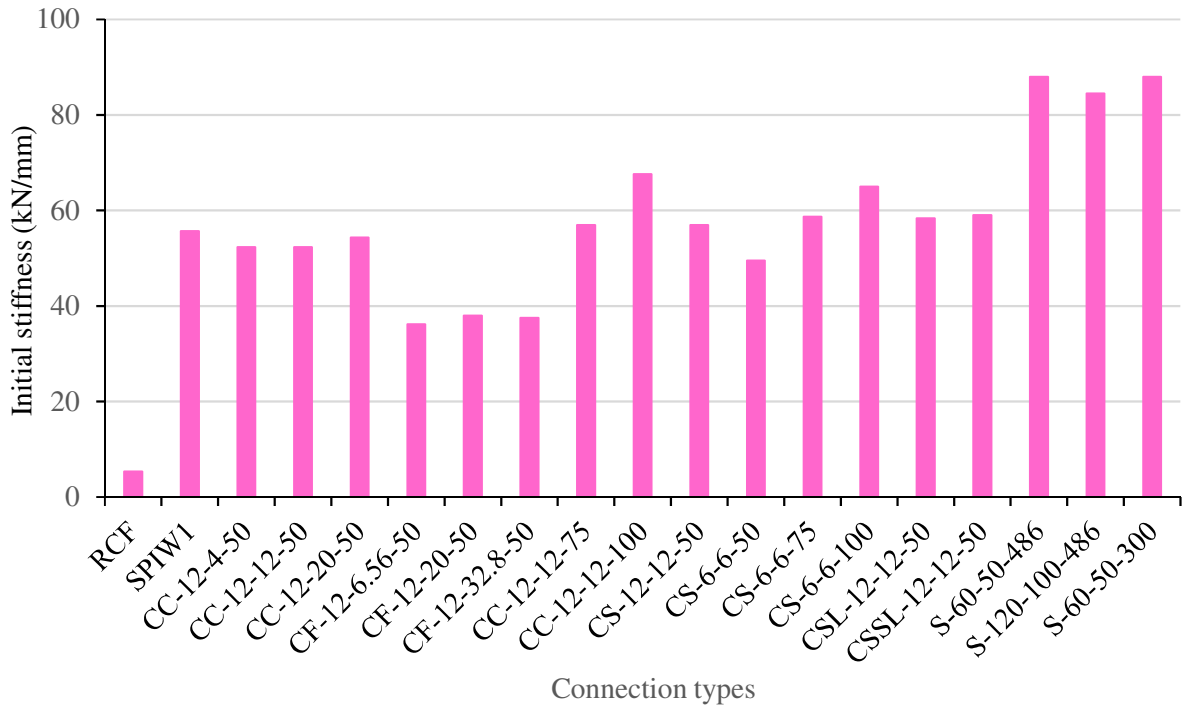

Fig. 20 Initial stiffness in all specimens

5. Conclusion

In this paper four connections for transferring the tension field forces between SPSW and RCF are proposed and investigated. Three of these connections are for rehabilitation of RC structures and one type is for new construction. Results of the specimens with different types of connections demonstrated that the use of SPSW in RCF with appropriate connections could provide excellent ductility as well as high load carrying capacity and initial stiffness by distributing the yielding zone in SPSW along the wall height (using the maximum capacity of the wall). Otherwise, if the connection does not have enough stiffness, the connection has a

large deformation and cannot transform the tension field forces of SPSW to RCF. This should be taken into account in rehabilitation of reinforced concrete structures with SPSW. The other obtained results are drawn as follows:

- Connections of the types 1-3, specimens CC, CF, CS, CSL and CSSL, are applicable for rehabilitation of RC structures; performance of this connections demonstrated that the use of CC and CS connections with the thickness ratio of L-section frame (connected to SPSW) to SPSW $(t_l/t_p) = 5$, are more desirable. In the connections type 3, CSL and CSSL specimens, placing the L-section profiles at the corners of the columns will not significantly affect the strength capacities compared to CS connection specimens (type 2) with similar conditions. Among these three types of connections, the use of CC and CS connections is preferable to CSL and CSSL connections. Among CC and CS connections by similar conditions, the use of CS connection is preferred. CS connection is the optimum connection method from the consumed steel volume point of view.
- The connections used for the experimental specimen (SPIW1) and S connection (Type 4) is applicable for new constructions. The results of initial stiffness, ductility and load carrying capacity of the specimens show that S connection has more appropriate performance compared to other specimens (including experimental). S connection, can be used as an appropriate method to connect SPSW to RCF.
- Investigations of this study demonstrated that instead of using the studs in beams and columns, use of the connection plates in beams and columns (type 1, CC and CF connection) with larger size (in this study for $(t_l/t_p) = 5$) of the L-section frame connected to SPSW could result in desired strength.

- The use of L-section profiles in corners of columns has no significant effect on increasing the system strength. Increasing the size of L-sections connected to SPSW is more effective for increasing the strength.
- Increasing the thickness of beam connection plates and plates of inside frame does not significantly increase the strength of specimens and causing to uneconomic connections. Increasing the size of the L-sections frame connected to SPSW is more effective to increase the strength.

References

[1] Council BSS. FEMA 356-Prestandard and Commentary for the Seismic Rehabilitation of Buildings. Washington DC: Federal Emergency Management Agency. 2000.
[2] Fukuyama H, Sugano S. Japanese seismic rehabilitation of concrete buildings after the Hyogoken-Nanbu Earthquake. Cement Concrete Comp. 2000;22:59-79.
[3] Kheyroddin A, Khalili A, Emami E, Sharbatdar MK. An innovative experimental method to upgrade performance of external weak RC joints using fused steel prop plus sheets. Steel Compos Struct. 2016;21:443-60.
[4] Sharbatdar MK, Kheyroddin A, Emami E. Cyclic performance of retrofitted reinforced concrete beam–column joints using steel prop. Constr Build Mater. 2012;36:287-94.
[5] Truong GT, Kim J-C, Choi K-K. Seismic performance of reinforced concrete columns retrofitted by various methods. Eng Struct. 2017;134:217-35.
[6] Badoux M, Jirsa JO. Steel bracing of RC frames for seismic retrofitting. J Struct Eng. 1990;116:55-74.
[7] Ghobarah A, Elfath HA. Rehabilitation of a reinforced concrete frame using eccentric steel bracing. Eng Struct. 2001;23:745-55.
[8] Youssef M, Ghaffarzadeh H, Nehdi M. Seismic performance of RC frames with concentric internal steel bracing. Eng Struct. 2007;29:1561-8.
[9] Sutcu F, Takeuchi T, Matsui R. Seismic retrofit design method for RC buildings using buckling-restrained braces and steel frames. J Constr Steel Res. 2014;101:304-13.
[10] Qu Z, Kishiki S, Maida Y, Sakata H, Wada A. Seismic responses of reinforced concrete frames with buckling restrained braces in zigzag configuration. Eng Struct. 2015;105:12-21.
[11] Almeida A, Ferreira R, Proença JM, Gago AS. Seismic retrofit of RC building structures with Buckling Restrained Braces. Eng Struct. 2017;130:14-22.
[12] Garcia R, Hajirasouliha I, Pilakoutas K. Seismic behaviour of deficient RC frames strengthened with CFRP composites. Eng Struct. 2010;32:3075-85.
[13] Zhu J-T, Wang X-L, Xu Z-D, Weng C-H. Experimental study on seismic behavior of RC frames strengthened with CFRP sheets. Compos Struct. 2011;93:1595-603.
[14] Ma C-K, Apandi NM, Sofrie CSY, Ng JH, Lo WH, Awang AZ et al. Repair and rehabilitation of concrete structures using confinement: A review. Constr Build Mater. 2017;133:502-15.
[15] AISC A. AISC 341-10, Seismic Provisions for Structural Steel Buildings. Chicago, American Institute of Steel Construction2010.
[16] CSA. S16-14, Design of Steel Structures. Canadian Standards Association, 2014.
[17] Sabelli R, Bruneau M. Steel plate shear walls (AISC design guide), American Institute of Steel Construction. Inc, Chicago, 2007.

[18] Zirakian T, Zhang J. Study on seismic retrofit of structures using SPSW systems and LYP steel material. Earthq Struct. 2016;10:1-23.
[19] Timler PA, Kulak GL. Experimental study of steel plate shear walls. 1983.
[20] Driver RG, Kulak GL, Kennedy DL, Elwi AE. Cyclic test of four-story steel plate shear wall. J Struct Eng. 1998;124:112-20.
[21] Elgaaly M. Thin steel plate shear walls behavior and analysis. Thin Wall Struct. 1998;32:151-80.
[22] Lubell AS, Prion HG, Ventura CE, Rezai M. Unstiffened steel plate shear wall performance under cyclic loading. J Struct Eng. 2000;126:453-60.
[23] Sabouri-Ghomi S, Ventura CE, Kharrazi MH. Shear analysis and design of ductile steel plate walls. J Struct Eng. 2005;131:878-89.
[24] Sabouri-Ghomi S, Gholhaki M. Tests of two three-story ductile steel plate shear walls. Structures Congress 2008:1-12.
[25] Choi I-R, Park H-G. Steel plate shear walls with various infill plate designs. J Struct Eng. 2009;135:785-96.
[26] Chen S-T, Jeng V, Chen S-J, Chen C-C. Seismic assessment and strengthening method of existing RC buildings in response to code revision. Earthquake Engineering and Engineering Seismology. 2001;3:67-77.
[27] Formisano A, De Matteis G, Mazzolani F. Numerical and experimental behaviour of a full-scale RC structure upgraded with steel and aluminium shear panels. Comput Struct. 2010;88:1348-60.
[28] Choi I-R, Park H-G. Cyclic loading test for reinforced concrete frame with thin steel infill plate. J Struct Eng. 2010;137:654-64.
[29] Görgülü T, Tama YS, Yilmaz S, Kaplan H, Ay Z. Strengthening of reinforced concrete structures with external steel shear walls. J Constr Steel Res. 2012;70:226-35.
[30] Committee A, Institute AC, Standardization IOf. Building code requirements for structural concrete (ACI 318-08) and commentary. American Concrete Institute; 2008.
[31] Abaqus 6.14–Analysis Users's Guide: Volume IV: Elements. 2013.
[32] Uang C-M. Establishing R (or R w) and C d factors for building seismic provisions. J Struct Eng. 1991;117:19-28.
[33] Newmark NM, Hall WJ. Earthquake spectra and design. Earth Syst Dynam. 1982.
[34] Krawinkler H, Nassar AA. Seismic design based on ductility and cumulative damage demands and capacities. Nonlinear seismic analysis and design of reinforced concrete buildings. 1992:23-39.
[35] Miranda E, Bertero VV. Evaluation of strength reduction factors for earthquake-resistant design. Earthq Spectra. 1994;10:357-79.
[36] Minimum design loads for buildings and other structures. Reston, Virginia: ASCE. American Society of Civil Engineers 2010.
[37] Provisions BPoISS, Agency USFEM. NEHRP Recommended Provisions for Seismic Regulations for New Buildings and Other Structures: Provisions: FEMA-450; 2003.